PHYSICAL REVIEW E **72**, 045104(R) (2005)

Complex dynamics in unidirectionally coupled overdamped bistable systems subject to a time-periodic external signal

Visarath In,[1,*] Adi R. Bulsara,[1,†] Antonio Palacios,[2,‡] Patrick Longhini,[2] and Andy Kho[1]
[1]*Space and Naval Warfare Systems Center, Code 2363, 53560 Hull Street, San Diego, California 92152-5001, USA*
[2]*Nonlinear Dynamics Group, Department of Mathematics, San Diego State University, San Diego, California 92182, USA*
(Received 8 July 2005; published 25 October 2005)

Recently, we have studied the emergence of oscillatory behavior in overdamped undriven nonlinear dynamic systems subject to carefully crafted coupling schemes and operating conditions [V. In *et al.*, Phys. Rev. E **68**, 045102(R) (2003).] The theoretical ideas have been validated in an experimental setup of $N=3$ coupled ferromagnetic cores subject to a dc external magnetic "target" signal; the oscillations (corresponding to the periodic switching of each core between its stable steady states of magnetization) are triggered when the coupling constant crosses a threshold value, with the oscillation frequency exhibiting a characteristic scaling behavior with the "separation" of the coupling constant from its threshold value, as well as with the external signal amplitude. Here, we consider the system response to a time-periodic signal. We demonstrate *experimentally* that, depending on the signal amplitude and frequency, the response can be either synchronized to the signal frequency or to one-third this frequency. These phenomena afford unique techniques for time-periodic signal detection and characterization for a large class of sensors.

DOI: 10.1103/PhysRevE.72.045104 PACS number(s): 02.50.Ey, 05.40.−a, 85.25.Dq

Well-designed coupling schemes, together with the appropriate choice of initial conditions, can induce oscillations in overdamped dynamical systems when a control parameter exceeds a threshold value [1]. We have demonstrated this behavior in a specific prototype system: three unidirectionally coupled ferromagnetic cores, the basis of a coupled core fluxgate magnetometer, with readout in the time domain [3] that is used to detect dc magnetic flux signals. Our analysis showed that N (taken to be odd, although the oscillatory behavior is also seen for N large and even) unidirectionally coupled elements with cyclic boundary conditions would, in fact, oscillate when a control parameter—in this case the coupling strength—exceeded a critical value. Note that energy conservation dictates that at least one of the elements must have an initial state different from the others for the oscillations to occur. The oscillations (corresponding to switching events between the stable magnetization states of each core) have been exploited to detect very weak "target" dc magnetic signals, via their effect on the oscillation characteristics. It is important to stress that this behavior is quite general; it has been demonstrated in coupled overdamped Duffing elements [1], and applied to the analyses of the frequency selective properties of interacting neural networks [4]. The emergent oscillations, which can be controlled by adjusting the system parameters, open up possibilities for the exploitation of a large class of (normally) nonoscillatory systems for a variety of practical applications that involve using the emergent oscillations as a reference.

In this work, we explore the response of our prototype coupled core magnetometer system to a time-periodic magnetic-flux signal, applied to each element in the array; effectively, we introduce another frequency (in addition to the network oscillation frequency in the absence of the signal) into the dynamics. The coupled system response then shows a richness of dynamical behaviors not seen in its single driven counterpart. We stress, however, that multistability and the response of one-dimensional (1D) nonlinear systems to time-periodic external signals have been studied in the past [2]. We now describe this behavior, starting with the dynamics [1] for three unidirectionally (cyclically) coupled flux-gate magnetometers,

$$\tau \dot{x}_i = -x_i + \tanh(c[x_i + \lambda x_{i+1} + h(t)]), \tag{1}$$

where τ is the device time constant; $x_i(t)$ represents the (suitably normalized) magnetic flux at the output (i.e., in the secondary coil) of unit i, where $i=1,2,3$, mod 3, and $h(t)=\varepsilon \sin \omega t$ is an externally applied "target" magnetic flux ($\varepsilon \ll U_0$), with U_0 being the energy barrier height (absent the coupling) for each of the elements (assumed identical for theoretical purposes). The individual dynamics in (1) are derived via a mean-field description of the domain dynamics in each ferromgnetic core; effectively, the core is treated as a "single-domain" entity. The individual potential functions for each element are bistable for $c>1$, with c being a temperature-dependent system parameter [3]. With a dc applied signal [$h(t)=\varepsilon$], the bifurcation to oscillatory behavior occurs at a critical coupling given (for $\tau=1$) by $\lambda_c=-\varepsilon+\lambda_0$ [1], where $\lambda_0=(1/c)\ln(\sqrt{c}+\sqrt{c-1})-\tanh[\ln(\sqrt{c}+\sqrt{c-1})]$; note that in our convention, $\lambda<0$ so that oscillations occur for $|\lambda|>|\lambda_c|$. The individual elemental oscillations are separated in phase by $2\pi/N$, and have period $T_i=[N\pi/(c(c-1))^{1/4}][1/\sqrt{\lambda_c-\lambda}+1/\sqrt{\lambda_c-\lambda+2\varepsilon}]$; these oscillations can be experimentally produced at frequencies ranging from a few Hz to high kHz and are, *always*, *supra*threshold, i.e., they correspond to switching events between the stable steady states of each core. While the oscillations occur [1] even for

*Electronic address: visarath@spawar.navy.mil
†Electronic address: bulsara@spawar.navy.mil
‡Electronic address: palacios@euler.sdsu.edu

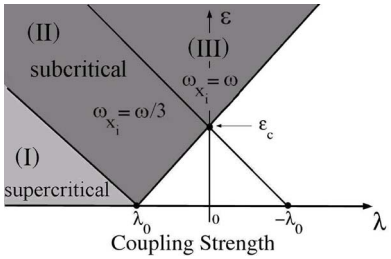

FIG. 1. (Color online) Theoretical phase diagram: Oscillatory behavior of the coupled flux-gate model (1) in parameter space (λ, ε). In the supercritical regime, the oscillations form a traveling wave pattern. In the subcritical regime, with $h(t)$ small, the system oscillates about one of the steady states ± 1, while with $h(t)$ large, the system oscillates between two steady states. In both cases the oscillations form a traveling wave and their frequency is exactly $\omega/3$. For ε greater than a critical value, all three waves are in phase with each other and frequency synchronized with the external signal $h(t)$ in region (III). Note that $\lambda_0 < 0$ in our convention (see text).

$h(t)=0$, their characteristics change when $h(t) \neq 0$; these changes can be exploited for signal quantification purposes.

Numerically integrating the system (1), with nonidentical initial conditions and $h(t)=\varepsilon \sin \omega t$, reveals three distinctive regimes of oscillatory behavior that are clearly separated (Fig. 1) in the parameter space (λ, ε):

(I) The *supercritical* regime wherein the coupling parameter is below the critical value ($\lambda < \lambda_0$, i.e., $|\lambda| > |\lambda_0|$ in our convention). In this regime, the coupled system oscillates with a traveling wave pattern as described above, even for $h(t)=\varepsilon$. In the presence of the target signal $h(t)$, the system responds by oscillating asymmetrically between the two stable magnetization states of each element. The response displays a frequency mixing (Fig. 2) of the inherent oscillations of the coupled system and the target signal. The bifurcation diagram (not shown) in this regime is quite complex ranging from the simple oscillations [for $h(t)=0$], to quasiperiodicity and, eventually, to chaos.

(II) The *subcritical* regime wherein the coupling strength exceeds the critical value ($\lambda > \lambda_0$, $|\lambda| < |\lambda_0|$), so that there are no spontaneous oscillations. For small $h(t)$, the system oscillates weakly (with no interwell switching) about the steady states near ± 1. With sufficiently large $h(t)$, the system oscillates between the two steady states in a traveling wave pattern where the amplitude and frequency of each oscillation are the same but a phase shift of $2\pi/3$ ($2\pi/N$ for odd N, in general) exists between the different wave forms. This behavior is quite similar to that already observed for the case of dc (or zero) target signal; however, the onset of the oscillations occurs sooner in parameter space when the applied signal is time periodic. The oscillation frequency is exactly $\omega/3$ (ω/N in general).

(III) Frequency matching of the output wave form to that of the target signal. With the control parameter λ held constant in the subcritical regime, increasing ε past a critical value causes the coupled system to switch to another oscillation mode wherein the frequency of the output wave form precisely matches that of the target signal. For weak signal detection purposes, the subcritical regime is more relevant

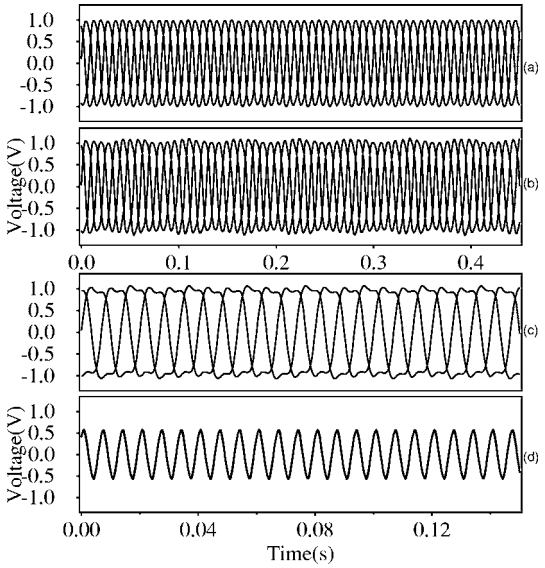

FIG. 2. Oscillation wave forms associated with the different regimes in the *experimental* system. (a) System (emergent) oscillations (at 44 Hz) in the supercritical regime (see Fig. 1) without an external field. (b) Characteristic modulation of the oscillations in the supercritical regime with a small applied ac magnetic-flux signal (at 150 Hz). (c) Oscillations in the subcritical regime where the system oscillates at $\omega/3$ (50 Hz) with no modulation of the wave forms. (d) Oscillations in phase with each other and frequency locked to the external signal. The external signal amplitude ε increases from panels (a) to (d). Each core response is transduced from a core magnetization to a (easily measured) voltage output (see [1] for details).

since it is relatively easy to extract information about the target signal via the residence times detection (RTD) method [1,3], because of the simplicity of the oscillation characteristics, e.g., constant amplitudes, frequencies, and phases; the RTD technique is not, however, easy to use in the supercritical regime.

We first consider the, more interesting, subcritical regime. We begin with an analytic calculation of the critical coupling strengths for the onset of the oscillations as function of the target signal amplitude ε and frequency ω. These results afford us the capability to set the boundaries, in parameter space, of the different types of oscillation characteristics in the subcritical regime (Fig. 1).

For a given ω and moderate values of (λ, ε) above the boundary line for the supercritical regime, each element oscillates at $\frac{1}{3}\omega$, with an interelement phase difference of $2\pi/3$. When the amplitude is large enough, the oscillations switch to an in-phase pattern with a frequency perfectly matched to the external signal frequency. This out-of-phase region is bounded (Fig. 1) by the supercritical region (below) and the in-phase region (above). To the right, the region is bounded by the line connecting $-\lambda_0$ and the critical signal amplitude ε_c, where the entrainment between the uncoupled $(\lambda=0)$ system and the external signal occurs. So the critical coupling $\lambda_{c_{sub}}$ for the onset of the oscillations, for a given ε, is

$$\lambda_{c_{sub}} = \lambda_0 - \left(\frac{\lambda_0}{\varepsilon_c}\right)\varepsilon. \tag{2}$$

Our strategy for finding an analytical expression for $\lambda_{c_{sub}}$ rests, therefore, on the ability to compute the critical value ε_c. Noting that the critical value ε_c corresponds to zero coupling (Fig. 1), we start with the reduced elemental dynamics

$$\tau\dot{x} = -x + \tanh[c(x + \varepsilon \sin \omega t)]. \tag{3}$$

The change of variable $y=x+\varepsilon \sin(\omega t)$ with rescaling and relabeling time using $\omega t+\phi=\omega t+\cos^{-1}(1/\sqrt{1+\omega^2\tau^2})$, allows us to transform (3) into the more convenient form

$$\dot{y} = -y + \tanh(cy) + \tilde{\varepsilon}\sin(\omega t), \tag{4}$$

where $\tilde{\varepsilon}=\varepsilon\sqrt{1+\omega^2\tau^2}$. Next we approximate $-y+\tanh(cy)$ near $y=1$, which is one of the equilibrium (magnetization steady-state) points, with a second-order polynomial $d+by+ay^2$, where a, b, and d are constant parameters that depend on the nonlinearity parameter c, and can be found via a Taylor expansion about $y=1$,

$$a = \frac{(4c^2 - 4c^2e^{2c})e^{2c}}{(e^{2c}+1)^3},$$

$$b = \frac{(-3+4c-8c^2)e^{2c} + (-3+4c+8c^2)e^{4c} - e^{6c} - 1}{(e^{2c}+1)^3},$$

$$d = -(a+b) + \left(\frac{e^{2c}-1}{e^{2c}+1} - 1\right). \tag{5}$$

We then seek an asymptotic solution of the form $y=y_0+\tilde{\varepsilon}y_1+\mathbf{O}(\tilde{\varepsilon}^2)$, to the simplified dynamics $\dot{y}=d+by+ay^2+\tilde{\varepsilon}\sin(\omega t)$. Substitution readily yields the system

$$\dot{y}_0 = d + by_0 + ay_0^2, \tag{6}$$

$$\dot{y}_1 = (b + 2ay_0)y_1 + \sin(\omega t), \tag{7}$$

which we now solve. The unperturbed problem (6) is a Ricatti equation, which we solve using a three-step standard approach: (i) search for a particular solution $y_0=A(a,b,d)$. Direct substitution into (6) yields $A=(-b-\sqrt{b^2-4ad})/2a$, where (b^2-4ad) must be non-negative. (ii) Use the change of variable $y_0=A+u$ to transform the Ricatti equation into a Bernoulli equation in u, given by $\dot{u}=(a+2aA)u+au^2$. (iii) Transform the Bernoulli equation into a first-order linear differential equation by substituting $w=1/u$, which yields $\dot{w}=-a-(a+2aA)w$. This linear equation can be readily solved following which back substitution into u and, in turn, into y_0 leads to

$$y_0(t) = A + \frac{1}{C_1 e^{-(b+2aA)} - \dfrac{a}{(b+2aA)}}, \tag{8}$$

where $C_1=a/(b+2aA)+1/[y_0(0)-A]$. Direct substitution of y_0 into (7), and using standard methods, yields a complete solution for y_1 given by

$$y_1(t) = \frac{C_2 e^{(b+2aA)t}}{\left[C_1 - \dfrac{a}{b+2aA}e^{(b+2aA)t}\right]^2} - \frac{\sin(wt+\phi)}{\sqrt{(b+2aA)^2+\omega^2}}, \tag{9}$$

where $C_2=y_1(0)[C_1-a/(b+2aA)]^2$. Combining (8) and (9) yields a complete solution, up to order $\mathbf{O}(\tilde{\varepsilon}^2)$, of (4), whence it can be shown that the asymptotic behavior of the original variable x is

$$\lim_{t\to\infty} x(t) = A - \left(\frac{\sqrt{1+\omega^2\tau^2}}{\sqrt{(b+2aA)^2+\omega^2\tau^2}} + 1\right)\varepsilon \sin(\omega t). \tag{10}$$

At the critical amplitude, ε_c, the non-zero-mean periodic solution $x(t)$ merges into a zero-mean periodic solution. This occurs when

$$\varepsilon_c = \frac{A\sqrt{(b+2aA)^2+\omega^2\tau^2}}{\sqrt{1+\omega^2\tau^2}+\sqrt{(b+2aA)^2+\omega^2\tau^2}}. \tag{11}$$

For the supercritical case one can, analogous to (2), write down (see Fig. 1)

$$\lambda_{c_{sup}} = \lambda_0 + \left(\frac{\lambda_0}{\varepsilon_c}\right)\varepsilon. \tag{12}$$

We have validated our theoretical results via an experiment consisting of three coupled ferromagnetic cores. The experimental setup is similar to the previously described case for dc target field detection [1]; hence, details of the coupling circuitry and the construction of the flux gates are not reproduced there. The system's behaviors (Fig. 2) agree well with the theoretical predictions. In the experimental run, the system is set up with the coupling strength in the supercritical regime so that it is oscillating (44 Hz) without any applied external field (top panel of Fig. 2). The next panel illustrates the modulation of the oscillation wave forms by a small amplitude ac external signal (at 150 Hz) while the system is still in the supercritical regime; note that the the system remains oscillating at the natural frequency (44 Hz). Thereafter, increasing the amplitude of the ac signal pushes the coupled system into the subcritical regime (see Fig. 1), and the resulting oscillations occur [panel (c) of Fig. 2] at $\frac{1}{3}$ the frequency of the ac signal without the amplitude modulation of panel (b). The last panel illustrates the case when the ac signal amplitude is increased sufficiently [into region (III)] so that the system switches to another behavior in the subcritical regime where all three wave forms are phase locked to each other and the oscillation frequency exactly matches that of the external signal. All four scenarios, illustrated here, have been predicted by theory, as illustrated in Fig. 1 and verified in numerical simulations (not shown).

Figure 3 provides experimental confirmation of the various oscillation regimes (of Fig. 1). The lines that separate the various regions are not quite as linear as those of Fig. 1, but the qualitative validation is evident. The slight inconsistencies arise, possibly from the device differences, because the ferromagnetic cores were nonidentical and their magnetic

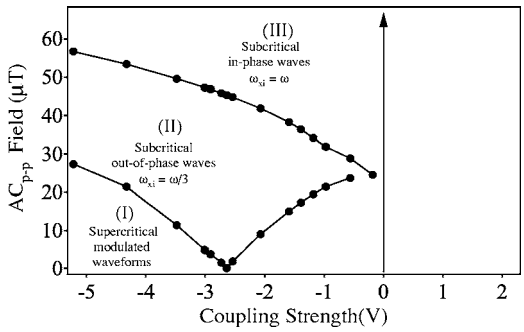

FIG. 3. Parameter space constructed via the *experimental* system, confirming the different oscillation regions theoretical predicted in Fig. 1. The coupling strength is expressed as a voltage, adjusted via a variable resistance. The applied signal is a 150-Hz magnetic field with varying amplitude.

domains were oriented differently. In addition, the coupling circuit components were nonidentical so that the coefficient λ was not the same for all the components of Eq. (1). Finally, there was a small dc voltage drift in the coupling circuitry which we could not completely remove.

Our previous work [1] demonstrated that unidirectional coupling and a judicious choice of initial conditions (that are, actually, the most natural for any experimental setup) can lead to oscillatory behavior in overdamped bistable systems even in the absence of an external forcing signal; in the presence of an additional dc target signal, the change in the oscillation characteristics has been exploited to characterize the target signal. The current work considers the emergent frequency-dependent phenomena when the coupled system is subject to a time-periodic external forcing. While a detailed analysis of each regime in Fig. 1 must be deferred to an upcoming paper, we note here the richness of behavior in different regimes of the parameter space of coupling and forcing signal amplitude; it is particularly noteworthy that the theoretical phase diagram has been validated experimentally and the experimental time-series response in the different regimes agrees with the results (not shown) of numerical simulations. The emergent behavior can be used to quantify time-periodic target signals, since the internal oscillation frequency (44 Hz in our setup) can usually be controlled by an appropriate choice of system parameters. The results of this work are expected to be applicable to a large class of nonlinear dynamic systems (of which our coupled micro-fluxgate system is only one example) coupled in this manner.

A.B. acknowledges support from the Office of Naval Research, under code 331. V.I. and A.K. acknowledge support from the Space and Naval Warfare Systems Center internal funding (S&T) program.

[1] V. In, A. R. Bulsara, A. Palacios, P. Longhini, A. Kho, J. D. Neff, Phys. Rev. E **68**, 045102(R) (2003); A. R. Bulsara, V. In, A. Kho, P. Longhini, A. Palacios, W.-J. Rappel, J. Acebron, S. Baglio, and B. Ando, *ibid.* **70**, 036103 (2004).

[2] P. Jung, G. Gray, R. Roy, and P. Mandel, Phys. Rev. Lett. **65**, 1873 (1990); T. Tome and M. de Oliveira, Phys. Rev. A **41**, 4251 (1990); M. Rao, H. R. Krishnamurthy, and R. Pandit, Phys. Rev. B **42**, 856 (1990); B. Chakravarty and M. Acharya Rev. Mod. Phys. **71**, 847 (1999); H. Fujisaka, H. Tutu, and P. A. Rikvold, Phys. Rev. E **63**, 036109 (2001).

[3] A. R. Bulsara, C. Seberino, L. Gammaitoni, M. F. Karlsson, B. Lundgvist, and J. W. C. Robinson, Phys. Rev. E **67**, 016120 (2003).

[4] V. In, A. Kho, J. A. Neff, A. Palacios, P. Longhini, and B. Meadows, Phys. Rev. Lett. **91**, 244101 (2003).